Effect of ultrasonic welding conditions and energy director thickness on structure and properties of lap-joints of PEEK-based composites reinforced with short carbon fibers

V.O. Alexenko, S.V. Panin, A.A. Zelenkov, D.G. Buslovich, L.A. Kornienko
Laboratory of Mechanics of Polymer Composite Materials, V.E. Panin Institute of Strength Physics and Materials Science of Siberian Branch of Russian Academy of Sciences, Tomsk, 634055, Russia
vl.aleksenko@mail.ru, http://orcid.org/0000-0003-4375-9132
svp@ispms.ru, http://orcid.org/0000-0001-7623-7360
alexeyzelenkov@yandex.ru, http://orcid.org/0009-0002-9331-8116
buslovich@ispms.ru, http://orcid.org/0000-0001-7464-9628
rosmc@ispms.ru, http://orcid.org/0000-0003-2064-9862

Lu Shaowei
School of Materials Science and Engineering, Shenyang Aerospace University, Shenyang, 110136, China
lushaowei_2005@163.com, https://orcid.org/0000-0003-2790-6753

ABSTRACT. The aim of this study was to investigate the effect of thickness of energy director (EDs) and ultrasonic welding (USW) process parameters on structure formation and interlaminar shear strength (LSS) values of lap-joints of composite polyetheretherketone (PEEK) based plates reinforced with 40 wt. % short carbon fibers (SCF). The null hypothesis was the necessity of complete melting and extrusion of the EDs from the fusion zones to ensure the minimal presence of discontinuities at reaching the maximum LSS value. During the USW with a flat anvil, frictional heating developed primarily along the periphery of the fusion zones due to less strict constraint conditions. The rational process parameters were the ED thickness of 100 μm and the USW duration of 800 ms, which enabled the formation of the fusion zones over the 62.5 % of the contact region. The LSS values of >11 MPa with the load at failure of >4500 N developed through the base material due to bending of the adherends. The use of a spherical anvil localized frictional heating and fusion in the center of the clamped region. Without EDs, the lap joints achieved the maximum stress at failure of >60 MPa; however, the small fusion zone area limited their load-bearing capacities to 3000 N. The multi-spot lap-joints of the adherends from the PEEK/SCF composite formed without EDs were

Citation: Alexenko, V.O., Panin, S.V., Zelenkov, A.A., Buslovich, D.G., Kornienko, L.A. Effect of ultrasonic welding conditions and energy director thickness on structure and properties of lap-joints of PEEK-based composites reinforced with short carbon fibers, Fracture and Structural Integrity, 77 (2026)281-297.

Received: 12.04.2026
Accepted: 17.05.2026
Published: 21.05.2026
Issue: 07.2026

characterized by the structural integrity, while the stress at failure was equal to ~30.8 MPa, which were 2–3 times higher than those with the EDs 100 and 250 μm thick. The structure of the multi-spot-welded joints was determined by the ratio of the ED thickness to the distances between adjacent spots. Inserting the EDs significantly enlarged the fusion zone area, but uneven distributions of the clamping force resulted in their different melting and spreading patterns, giving rise to in discontinuities in the formed structure. The optimization of USW procedures for fibrous PEEK/SCF composites should be aimed at achieving a balance between the distances between adjacent spots and the ED thickness to ensure control of melting the polymer in fusion zones (outside the clamped region) and to eliminate the formation of discontinuities caused by its deficiency due to squeezing out.

KEYWORDS. Ultrasonic welding, Polymer matrix composite, Polyetheretherketone, Short carbon fiber, Energy director, Interlaminar shear strength

INTRODUCTION

Up-to-date layered composites (laminates) based on polyetheretherketone (PEEK) reinforced with continuous carbon fibers (PEEK/CF laminates) exhibit improved strength properties, including at elevated temperatures, which contribute to their widespread use in the aerospace and other advanced industries [1,2]. As a thermoplastic polyether, PEEK is characterized by a melting point of ~343 °C and great chemical stability in aggressive environments [3] that expand its industrial applications in both car manufacturing and medicine [4]. Another distinctive feature of the PEEK-based composites is the ability to be multiply recycled due to their thermoplastic nature, distinguishing them from thermosetting matrices. However, heterogeneous structure of the interfaces between layers remains a key factor deteriorating their static and cyclic strengths [5]. Accordingly, such challenges have to be overcome in their manufacturing and subsequent joining of parts (if necessary). In these cases, ultrasonic welding (USW) is one of the most suitable techniques. This process involves applying US-vibrations of a working tool (sonotrode) to the surfaces of the parts to be welded under application of clamping force. As a result, they are locally heated and fused without significant (thermally induced) damage to the materials being joined [6, 7]. Typically, USW is implemented for thermoplastics and their composites due to i) high productivity, as well as ii) formation of few discontinuities and iii) low residual stresses in welded joints [8].

USW enables the formation of permanent joints of the PEEK/CF laminates (adherends), ensuring high strength properties while preserving their original structure [9]. The size of thermomechanically affected zones (TMAZs) can be minimized by inserting and melting consumable energy directors (EDs) in fusion zones. Another important task is the optimization of USW process parameters (amplitudes of US-vibrations, clamping forces and process durations), which determine the strength properties and durability of welded joints [10]. Its solution allows to improve the quality of the formed structures in the fusion zones of the PEEK/CF laminates. Accordingly, their application areas are widened due to the expansion of technological capabilities and reliability in accordance with operating conditions [11, 12].

In addition to the commonly used PEEK/CF laminates, some other PEEK-based composites are reinforced with short carbon fibers (SCFs) [13–15], which unfortunately have received little attention so far. For example, USW was applied for joining additively manufactured parts from PEEK and its composite containing 10 wt. % SCFs [16]. The effects of the shape and size of EDs, as well as USW process parameters on the strength properties of welded joints were assessed. It was found that the EDs with circled profiles and the optimized USW parameters (a clamping force of 250 N and an amplitude of US-vibrations of 40 μm) ensured the process stability and great load-bearing capacity (up to 1.97 kN at energies of 300–500 J). The most important result was the achievement of the cohesive fracture mode (i.e., outside the fusion zone), confirming the key role of the strength properties of the welded joints of the additively manufactured parts (comparing with the interlayer adhesion).

The formation of microreliefs on the surfaces of joined parts from the PEEK/CF composite (30 wt. % SCFs 200 μm long and 7.5 μm in diameter) localized heat generation in USW, increasing loads at failure of their welded joints by ~30 % (up

to ~8 kN) [17]. The optimal USW duration was 1.5 s for single-side surface microtexturing, which maintained the matrix integrity preventing its structural degradation. Shortening the USW duration to 1 s caused insufficient frictional heat generation for the formation of US-welded joints, while its prolonging to 2 s led to thermal degradation of the polymer, the presence of pores, and instability of the process.

In addition to the USW process parameters, the shape of elastic bases (the so-called anvils) greatly affects the formation of welded joints. Conventional flat anvils do not provide sufficient heat localization in most cases, resulting in uneven fusion of the welded parts and low strength properties of the formed joints. According to [18], the use of a ring-shaped anvil with a bearing diameter of 10 mm in USW of parts from the PEEK/CF composite (30 wt. % SCFs ~100 μm long) was more effective than a flat one due to its circular support zone, which concentrated energy and localized Coulomb friction. Thereby, heating and diffusion of the molten polymer accelerated improving the strength of the welded joint up to 7.4 MPa, which was 2.1 times higher than that for the flat anvil. However, excessive expansion of the support zone contributed to thermal degradation of the matrix, increasing porosity in the welded joints from 41.3 % up to 56.2 %. In turn, the authors of [19] proposed an alternative approach to performing USW without EDs by replacing typical flat anvils with spherical ones. They investigated the effects of both spherical tip radius and energy of US-vibrations on the structure and strength properties of welded joints of parts from the PEEK/CF composite (30 wt. % SCFs with a length of ~200 μm and a diameter of 7.5 μm). The use of the spherical anvil ensured efficient energy concentration, enhancing the structural homogeneity of the welded joints and minimizing the presence of discontinuities.

As noted above, there are still many knowledge gaps regarding USW of fibrous PEEK-based composites. In particular, patterns of the structure formation in fusion zones were not identified in terms of the interaction of consumable EDs with adherends, since the primary attention was focused on high-strength laminates (reinforced with fabrics or tapes of unidirectional continuous fibers) [20]. An important aspect is understanding the characteristics of energy transfer from US-vibrations towards fusion zones depending on the strength properties (elastic moduli) of the top adherend clamped with a sonotrode (for particulate composites, they are lower than those for continuous fiber reinforced ones).

The aim of this study was to investigate the effects of ED thicknesses and USW process parameters on the structure formation and interlaminar shear strengths of welded joints of a PEEK-based composite loaded with SCFs. The null hypothesis was the necessity of complete melting and extrusion of the EDs from the fusion zones to ensure the minimal presence of discontinuities at reaching the maximum shear strength.

MATERIALS AND METHODS

The components of the studied PEEK (60 wt. %)/SCF (40 wt. %) composite were preliminary compounded by dry mixing. The 770PF PEEK powder (China) with an average particle size of 50 μm was used as a matrix. It was dispersion mixed with as-received SCFs 2 mm long and 10 μm in diameter (ZUKM LLC, Chelyabinsk, Russia) that were without prior annealing, i.e., with a sizing agent on their surfaces (for epoxy binders). In this way, both PEEK powder particles and SCFs were dispersed using a Bosch paddle mixer (ErgoMixx, Robert Bosch GmbH, Germany) at a rotor speed of 12,500 rpm for 5 minutes. Then, the obtained mixture was placed into a mold to form 170×125×2 mm^3 adherends using a GT-7014-A 122 heat press (GOTECH Testing Machines Inc., Taiwan) at a temperature of 390 °C, a pressure of 10 MPa, and a holding time at the maximum temperature of 30 minutes.

The adherends were cut out from the composite plate using a 3-axis CNC vertical milling machine (NPO "Purelogic" LLC, Russia). A 2 mm diameter solid carbide vertical tool was employed for the operation. To ensure high-quality edges and minimize delamination, the following processing parameters were strictly maintained: Spindle speed – 15,000 rpm; Feed rate – 600 mm/min; Axial depth of cut – 0.5 mm. Following the machining process, the milled edges of the adherends were manually wet-polished using P1000-grit sandpaper. In accordance with ASTM D5868, the lap-joined adherends were prepared with dimensions of 100×20×2 mm^3.

The ED elements used in this study were commercially available polyetheretherketone (PEEK) films with thicknesses of 100 and 250 μm. These films were manufactured by Jilin Zhongyan High Performance Plastic (Changchun, China) under the brand name ZYPEEK.

USW was performed with a UZPS-7 machine (SpetsmashSonic LLC, Russia) at an amplitude of US-vibrations of 10 μm and a frequency of 20 kHz. When using a flat anvil, the dimensions of fusion zones of the joined adherends were 20×20 mm^2, determined by the sonotrode sizes according to Fig. 1, a.

The adherends were placed in a clamp, preventing their relative movement during USW (mode #1). According to previous research by the authors [21], uniform melting and spreading of EDs were virtually impossible to achieve with these sonotrode dimensions. Therefore, mode #2 was also utilized, namely, localized ("spot") USW using a spherical anvil (Fig. 1,

b). In this case, the welded joints were formed locally, since the fusion zones were frictionally heated only at the clamping area. This proposed USW procedure was rather a model one. On the one hand, it enabled to simulate the spot USW process, including for the subsequent development (outside the scope of this study) of a technique for the formation of welded joints with a sonotrode continuously moving relative to the adherends being joined [22]. On the other hand, since it was impossible to uniformly focus US vibrations over the area of 20×20 mm, an analysis of the structures in the spot-welded joints allowed to more accurately identify the specifics of the processes developing upon USW. Another trial option was a multi-spot USW procedure (mode #3; Fig. 1, c), which involved step-by-step discrete movement of the adherends relative to the apex of the spherical anvil. The applied USW parameters are presented in Tab. 1.

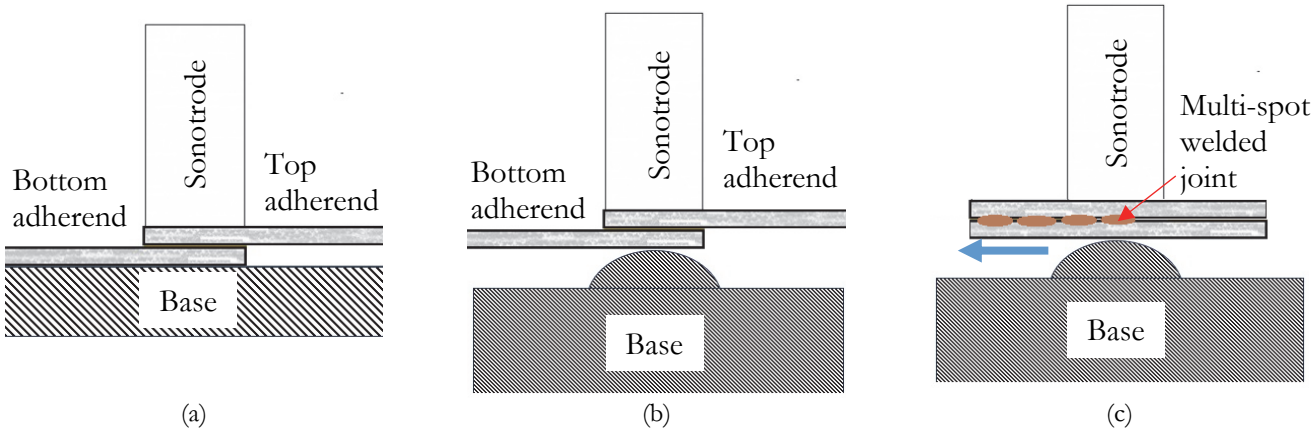

Figure 1: The USW diagrams for modes #1 (a), #2 (b) and #3 (c)

USW mode	USW duration, ms	Clamping force, atm	ED thicknesses, μm	Number of specimens
#1 flat anvil, conventional	800, 1000, 1200	1.7	0 (without EDs), 100, 250	5
#2 spherical anvil, single-spot	600, 800, 1000	1.0	0 (without EDs), 100, 250	5
#3 spherical anvil, multi-spot	800	1.0	0 (without EDs), spot pitch 4 mm 100, spot pitch 2 mm 250, spot pitch 4 mm	5

Table 1: The applied USW parameters

For mode #1, the experiment was planned according to the full factorial technique with two variable parameters (USW duration [t_{USW}, ms] and ED thickness [δ, μm]) at three levels, while the clamping force of 1.7 atm and the holding time after switching off US-vibrations of 2000 ms were constant. As shown below, the applied USW process parameters were suitable for joining the adherends only with the EDs. Considering this fact and lower required input energy, the clamping force was reduced down to 1 atm for mode #2.

Based on the results previously obtained by the authors in the aspect of the implementation of USW for joining adherends from neat PEEK with PEEK/CF fabric prepregs [23], the clamping force was set at the minimum possible level in this study (determined empirically in some trial experiments). The following considerations were taken into account: i) to minimize the damaging effect on the top adherend, which was cyclically subjected to the hammering action of the sonotrode; ii) to level out spreading of the molten EDs, since turbulent flows increased porosity; iii) the EDs were melted nonlinearly in time, so the clamping force reduction had to accelerate this process ensuring the formation of US-welded joints.

The lap shear strength (LSS) tests of the welded joints were conducted with an Instron 5582 electromechanical tensile testing machine at a cross head speed of 13 mm/min according to ASTM D5868. The LSS values were calculated using the following expression:

$$LSS = \frac{P}{F} \tag{1}$$

where P was the load at failure, N; F was the contact area of the joined adherends, mm².
The structures of the welded joints and their fracture surfaces were examined using a Neophot 2 optical microscope (OM; Carl Zeiss Jena, Germany) equipped with a Canon EOS 550D digital camera (Canon Inc., Japan) and an Apreo 2 S scanning electron microscope (SEM; Thermo Fisher Scientific, Waltham, MA, USA) at an accelerating voltage of 25 kV and a e-beam current of 0.80 nA.
To quantify the fusion zone area, a digital image analysis of the failed specimens was performed. The boundaries of the fusion zones, were manually traced, and the corresponding surface areas were calculated using ImageJ software (National Institutes of Health, USA). To calibrate the pixel scale to absolute units (mm²), a reference scale included in the original photographs was used. For each USW condition, measurements were conducted on all tested specimens to ensure statistical reliability and determine the average values with standard deviations.

EXPERIMENTAL RESULTS

Mode #1

Fig. 2 shows dependences of the LSS values and the loads at failure vs the USW durations for all nine combinations of the applied parameters (Tab. 1) without taking into account the fracture mechanisms. It should be noted that the welded joints failed via the interlaminar shear mechanism not in all cases. Therefore, if failure was through the base material (namely, due to bending of an adherend according to Fig. 3, b [23]), the actual LSS value was higher than that shown in Fig. 2.

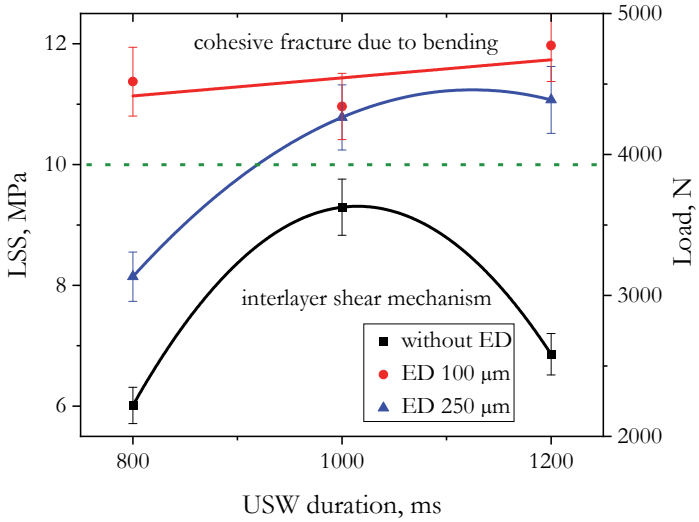

Figure 2: The dependences of the LSS values and the loads at failure on the USW durations; USW mode #1

(a) (b)

Figure 3: The OM images of the fractured USW-joints: along the fusion zone (by the interlayer shear mechanism) without EDs at t_{USW}=1000 ms (a) and along the base material (cohesive fracture due to bending) at δ=100 μm and t_{USW} =1000 ms (b); USW mode #1

The welded joints formed with the EDs failed due to bending outside the fusion zones along one of the adherends (through the base material), regardless of the USW duration. This fracture pattern was not reported previously in the literature on

USW of laminates, as their reinforcement with continuous CFs eliminated its [24]. The LSS values shown in Fig. 2 were proportional to the fusion zone areas (circled by red dotted lines in Fig. 4, a–c).

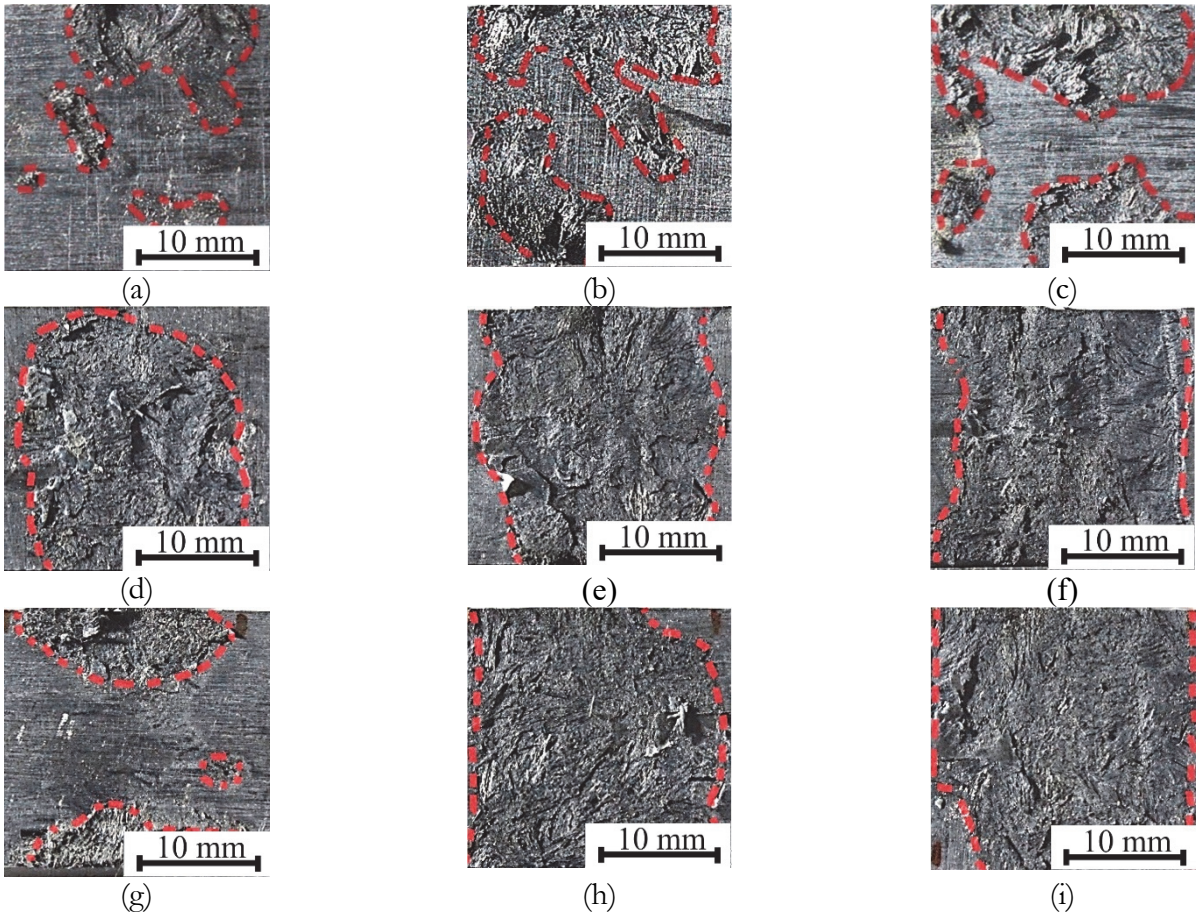

Figure 4: The OM images of the fracture surfaces; USW mode #1 without ED: a – t_{USW}=800 ms, b – t_{USW} =1000 ms, c – t_{USW} =1200 ms; δ=100 μm: d – t_{USW} =800 ms, e – t_{USW} =1000 ms, f – t_{USW} =1200 ms; δ=250 μm: g – t_{USW} =800 ms, h – t_{USW} =1000 ms, i – t_{USW} =1200 ms;for cases d), e), f), h), i) the samples were fractured manually (mechanically) after the LSS tests.

The welded joints formed without EDs failed via the interlaminar shear mechanism at all the applied USW durations. The maximum LSS value of ~9.3 MPa was achieved at t_{USW}=1000 ms, decreasing with its prolongation up to 1200 ms. This result was unexpected, since the generated frictional heat had to be increased with prolonging the USW duration. Consequently, melting of the polymer within the adherends being joined had to be enhanced enlarging the fusion area. However, this conclusion was more valid when using the EDs. Without them, excessive melting of the polymer matrix could damage the surface layers of the adherends. In any cases, the achieved LSS values were low compared to previously reported levels of ≥25 MPa [20, 25].

At δ=100 μm, all welded joints failed through the base material (Fig. 4, d–e), reflecting high interlayer adhesion levels. The LSS values (which were not actually considered as such due to the implementation of another fracture mechanism) were 11.5±0.5 MPa with the stresses at failure of ~115 MPa (Fig. 2), practically independent of the USW durations. Since macroscopic bending of the lap joints could not be completely eliminated in the LSS tests, the above-described spot ones were examined for understanding this parameter more objectively (the results are presented below).

Typically, the thicknesses of EDs used for USW of laminates did not exceed 250 μm [20], involving the formation of welded joints reinforced with CF fabrics or unidirectional continuous fibers. In this study, the EDs 250 μm thick were also inserted, which reduced the LSS values compared to those for δ=100 μm, all other things being equal (Fig. 2). At t_{USW}=800 ms, failure occurred through the fusion zones with the (expected low) LSS values of 8.1±0.6 MPa caused by their small areas (Figs. 4, f and 5). At longer USW durations, the welded joints failed through the base material apparently due to more complete melting of the polymer matrix in the surface layers of the adherends being joined (Figs. 4, h, i and 5) at the LSS values of 11.0±0.3 MPa and stress at failure of ~110 MPa.

As noted above, the fracture mode of the lap-joints (through the fusion zones or the base material) was determined by the interface area of the adherends being joined. This parameter was estimated based on the data presented in Figs. 4 and 5, a. Similar to Fig. 2, the graph in Fig. 5, a is divided into two regions characterized by different fracture mechanisms. These data indicated that the formation of the welded joints with the minimum acceptable LSS values was possible at the total fusion areas of ≥200 mm² (i.e., ≥50 % of that for the sonotrode size of 20×20 mm²).

According to the obtained results and previously reported data, thinning of the welded joints (measured integrally by the sonotrode displacement during USW, for example) was a suitable control parameter, a critical change of which could serve as an indicator for switching off US vibrations [20, 22, 23]. In this study, the authors also (integrally) assessed thinning of the welded joints after the USW. For this purpose, a mechanical micrometer was used, taking at least five measurements with subsequent averaging of the obtained values (Fig. 5, b). In these dependences, it was not possible to divide the results into two non-overlapping areas, as in the graphs shown in Figs. 2 and 5 (due to uneven thinning of the welded joints across the fusion zone areas, among other things).

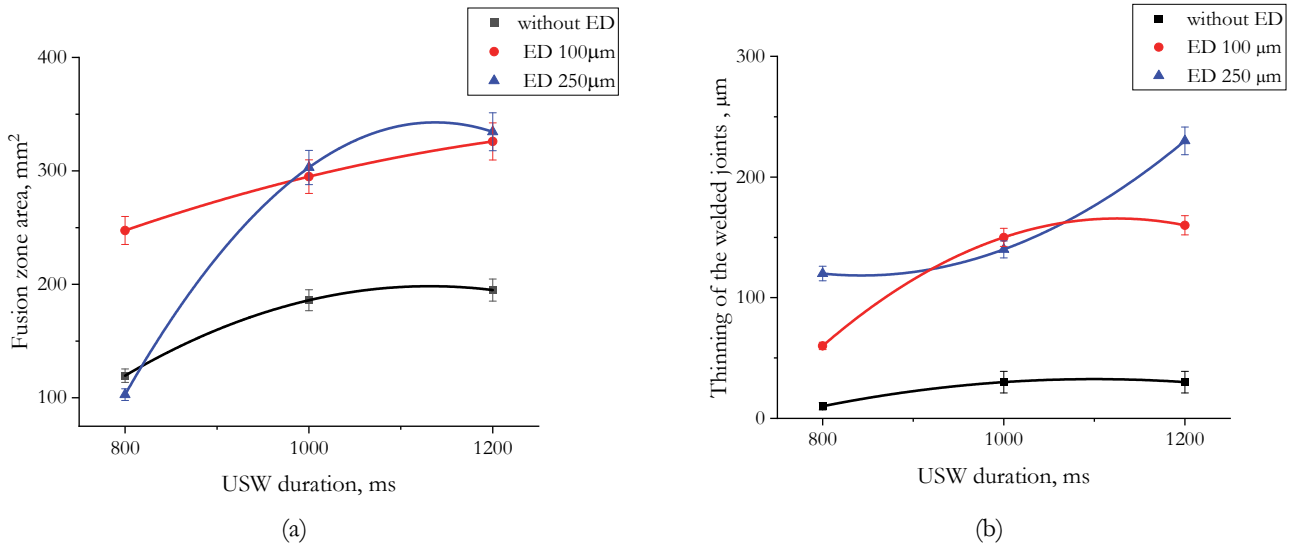

Figure 5: The dependences of the fusion zone areas (a) and thinning of the welded joints (b) on the USW durations; USW mode #1.

The dependences presented in Fig. 5, b are to be analyzed taking into account the initial thicknesses of the inserted EDs (or their absence). In the latter cases, thinning of the welded joints occurred due to (partial) melting of the polymer matrix in the surface layers of the adherends. Thus, the fracture surfaces shown in Fig. 4, a–c could visualize the development of the melting processes at the interfaces. According to Fig. 4, c, the depth of cohesive fracture traces (via tearing out of fragments) within the fusion zones increased with prolonging the USW durations. At the same time, both fusion zone areas and thinning of the welded joints were virtually identical at 1000 and 1200 ms. Melting in the center of the interfaces between the adherends did not occur (or was minimal) regardless of the USW durations. This phenomenon could be caused by the fact that the fusion zone perimeters was less constraint fixed during the USW, since the outer edges of the adherends were not rigidly attached to the sonotrode.

At δ=100 μm and t_{USW}=800 ms, thinning of the welded joint was half the initial ED thickness (Fig. 5, b) with a fusion zone area of ≥250 mm². These conditions were sufficient to achieve the acceptable LSS value (Fig. 2). With prolonging the USW duration, thinning of the welded joint tripled (up to 150 μm), amounting to one and a half ED thicknesses. Since this phenomenon would be accompanied by melting of the adherends being joined, the implementation of these USW durations could be impractical.

For the thick ED (δ=250 μm), thinning of the welded joint was ~120 μm (approximately half of the initial ED thickness; Fig. 5, b) at the minimum USW duration of 800 ms. Fusion zones were observed only in two triangular-shaped regions located along the lateral faces of the welded joint (Fig. 4, g), which were characterized by the minimal clamping force during the USW. According to the authors, the ED was melted more intensively due to its facilitated mutual sliding (friction) with the joined adherends. Nevertheless, the fusion zone area was insufficient to achieve the acceptable LSS value (Fig. 2). With prolonging the USW durations to 1000 and 1200 ms, thinning of the welded joints increased nonlinearly, reaching ~240 μm in the latter case, that was comparable to the initial ED thickness (Fig. 5, b). This result, however, was not accompanied by

neither a noticeable increase in the fusion zone areas (Fig. 5, a) nor the LSS values (as noted above, the fracture mechanism differed from the interlaminar shear in these cases).
The obtained results enabled to draw the following preliminary conclusions:
- melting of the EDs was determined by their thicknesses and USW durations, but developed unevenly, both in time and space;
- extrusion of the molten EDs could occur at the edges of the fusion zones only (to the periphery); the melt flow process had to develop unevenly and be accompanied by the formation of discontinuities, pores, and changes in the thickness of the solidified material;
- during USW of the adherends from the particulate composite, melting of both their surface layers and the EDs was possible, accompanied by their mixing.
These considerations necessitated conducting the structural studies, taking into account the above-identified patterns of changes in the mechanical properties and macrostructural characteristics (in particular, thinning of the welded joints).
Fig. 6, a shows the structure of the welded joint obtained at δ=100 μm and t_{USW}=800 ms, while some images captured at a higher magnification in the center and closer to the fusion zone edge are presented in Fig. 6, b–d. In the center, the ED was not melted practically (Fig. 6, b) and the adherends were damaged minimally (Fig. 6, a, left). Closer to the edges, melting of the ED was expressed to a greater extent (Fig. 6, c). Accordingly, spreading of the molten ED was accompanied by the formation of defects, predominantly located in the top adherend (since it transferred the energy of US vibrations into the fusion zone).

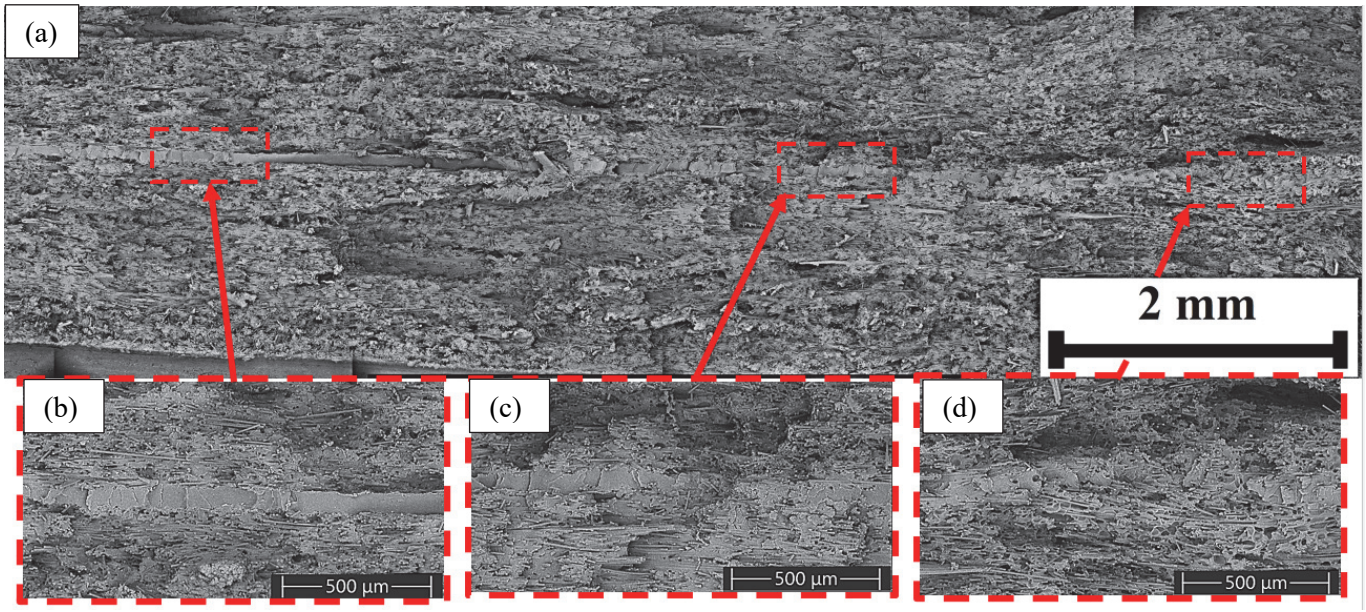

Figure 6: The SEM micrographs of the structure of the USW-joint at δ=100 μm and t_{USW}=800 ms; USW mode #1.

Closer to the fusion zone edge, the original ED structure changed significantly. The reason was the fact that it was melted to its maximum extent in this region (Fig. 6, b). Nevertheless, the molten ED was also extruded here from the central part, accompanied by plastic flow and intense mixing. As a result, the structure was defective and less uniform.
According to Fig. 6, a, partial melting of the ED 100 μm thick occurred only in the central part of the fusion zone, while it was extruded and spread closer to the edges. Due to the negligible ED thickness, the polymer extruded toward the periphery was not damaged greatly the surface layers of the adherends (as at δ=250 μm, see Fig. 7, a below).
For the thick ED (δ=250 μm), the patterns of the structural changes differed, especially at the fusion zone periphery (Fig. 7, a). At the center of the welded joint, the ED was also melted minimally (Fig. 7, b). The adherends were reliably joined with the minimum number of damages and discontinuities near the fusion zone. At greater distances from the center, the ED's melting intensity increased (accompanied by local thinning, Fig. 7, c). Some visible extended defects in the bottom adherend (Fig. 7, a, bottom center) were unlikely caused by manual chipping of the sample for the structural examinations after exposure to liquid nitrogen, but not due to melting and spreading of the ED in USW.
In a region adjacent to the edge of the welded joint, the structure was highly heterogeneous (Fig. 7, d), as in the previous case. Spreading of the molten ED was accompanied by its mixing with the surface layers of the adherends. At the very edge

of the fusion zone, the polymer flow was so intense that it significantly damaged the structural integrity of the welded joint (Fig. 7, a, right).

Unlike USW of laminates reinforced with CF fabrics, when thinning the welded joints by the ED thickness was the criterion for switching off US-vibrations to achieve the highest LSS values [20], it was not applicable for the particulate composites in all the studied cases. The use of the ED 100 μm thick enabled to minimize damage to the welded joints, achieving higher strength properties in the USW mode #1.

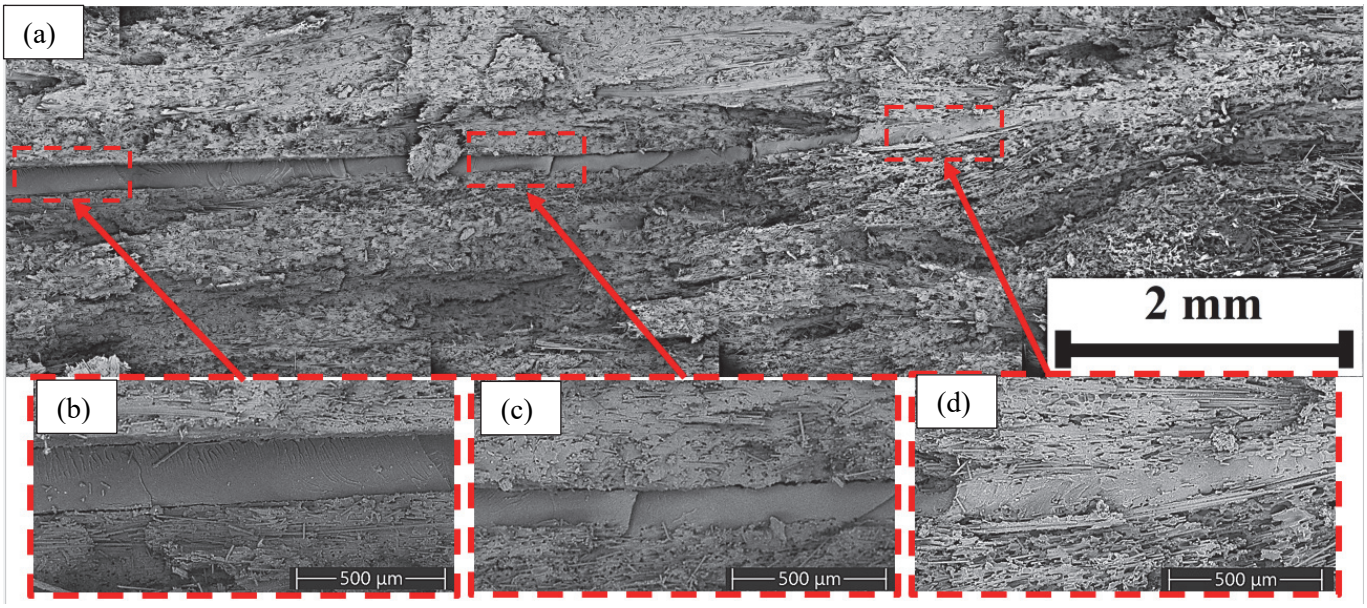

Figure 7: The SEM micrographs of the structure of the USW-joint at δ=250 μm and t_{USW}=800 ms; USW mode #1.

USW mode #2

Since the patterns of the structure formation during USW with the flat sonotrode were affected by the numerous factors (often in opposite ways), USW mode #2 was tested additionally with the variable parameters presented in Tab. 1. Fig. 8 shows the results of evaluating both LSS values and load at failure of the obtained welded joints. It should be noted that smaller areas of the fusion zones made it possible to shorten the range of the USW durations to 600–1000 ms and to decrease the clamping force down to 1 atm. When calculating the LSS values, the measured stresses at failure were normalized to the actual areas of the fusion zones (Fig. 9). All these welded joints failed according to the interlaminar shear mechanism.

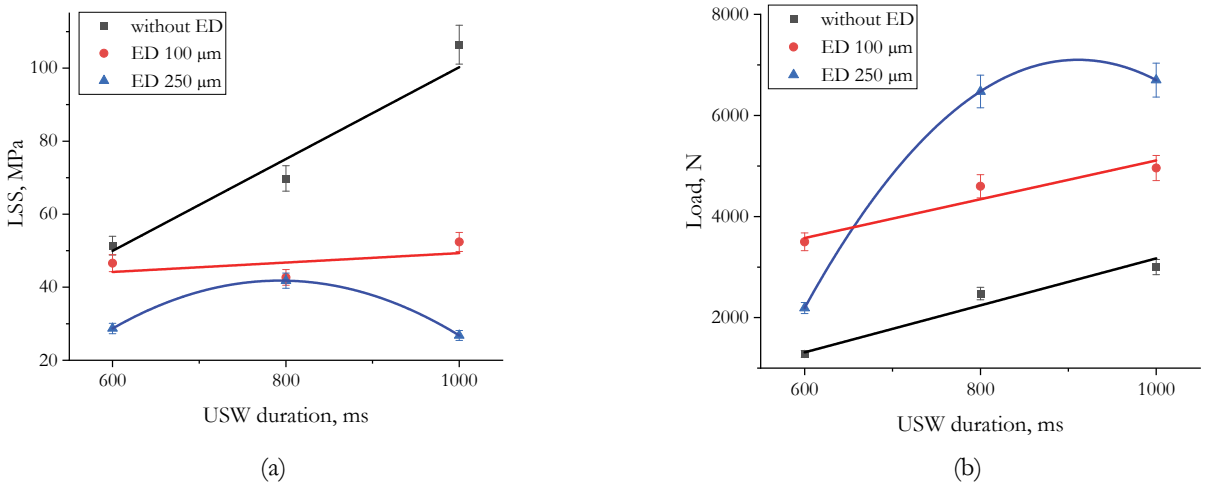

Figure 8: The dependences of the LSS values (a) and the loads at failure (b) vs the USW durations; USW mode #2

For the US-welded joints formed without EDs, a linear correlation was characteristic between the USW durations and the LSS values. Its maximum level of ~106 MPa was achieved at t_{USW}=1000 ms, while the load at failure of about 3000 N was relatively low (Fig. 8, b). When using the EDs 100 μm thick, the same dependence was rather extreme. The peak LSS value of 52 MPa was also recorded at t_{USW}=1000 ms, but a significant increase in the load at failure up to 4900 N was observed (comparing to the previous cases). At δ=250 μm, the optimal USW duration shortened: the LSS value of ~41 MPa was maximum at t_{USW}=800 ms, while the strength properties decreased then. Despite the lower LSS values, this group of the welded joints showed the highest load-bearing capacity, since the load at failure exceeded 6000 N (Fig. 8, b).

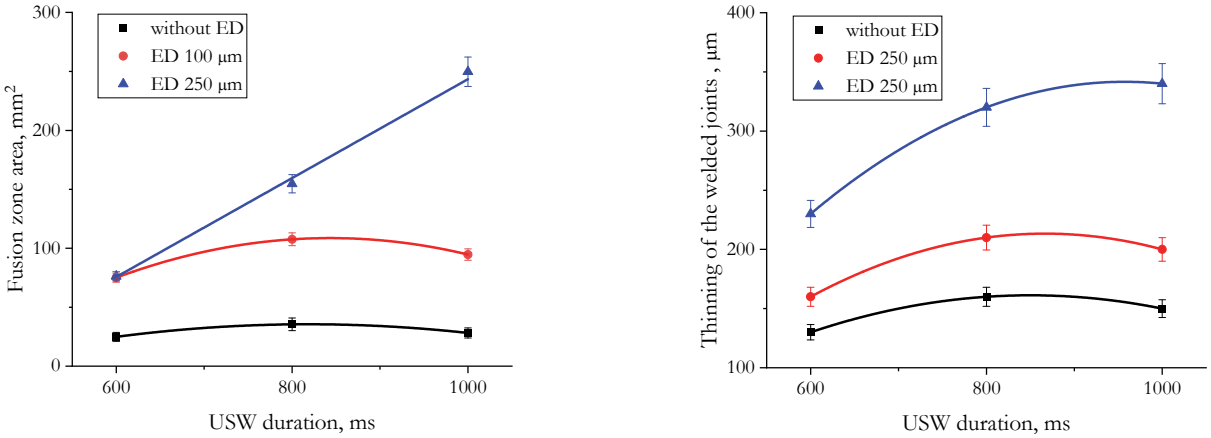

Figure 9: The dependences of the fusion zone areas (a) and thinning of the welded joints (b)vs the USW durations; USW mode #2

The differences in the obtained results were caused by variations in the fusion zone areas depending on the USW durations (Fig. 9, a). The welded joints without EDs and with one 100 μm thick exhibited identical character: the maximum fusion zone areas were at t_{USW}=800 ms (35 and 107 mm², respectively), but they decreased at t_{USW}=1000 ms. For the thick EDs (δ=250 μm), the trend changed to an upward one: the fusion zone areas enlarged monotonically in the entire range of the USW durations, reaching their maximum of 250 mm² at t_{USW}=1000 ms. It should be emphasized that the maximum loads at failure and the fusion zone areas were enhanced up to the acceptable levels at δ=250 μm, as determined previously using the flat anvil. However, none of the welded joints failed through the base material, as their width was 30 mm (but not 20 mm as in USW mode #1) to prevent the development of the edge heating effect when using the spherical anvil.

Fig. 9, b shows thinning of the welded joints measured at their centers. The obtained data differed somewhat from the values typical for the flat anvil, but retained the general trend (the longer USW duration, the thinner the welded joint). Without EDs, the maximum thinning of the welded joints was 160 μm. At δ= μm, it increased up to 210 μm, reaching 340 μm at δ=250 μm. In all the studied cases, the peak thinning values were caused by deformation and fracture of the base material (adherends).

OM images of the fracture surfaces (Fig. 10) represent the spot-welded joints that reflected the shape of the spherical anvil. Unlike the flat analog, which resulted in island-like melting, the spherical anvil localized the maximum clamping areas at its center, ensuring the radial fusion zones.

Without the EDs, the sphere apex was heated maximally, resulting in the smallest fusion zones characterized by the adhesive fracture mechanism (Fig. 10, a–c). At δ=100 μm, the fusion zone areas increased proportionally with prolonging the USW durations, and the fracture mechanism changed to a mixed one. In the latter case the centers of the fusion zones were subjected to intense plastic deformation of the matrix due to the viscous flow of the molten polymer matrix (Fig. 10, d–f). With the thick EDs (δ=250 μm), the largest fusion zone areas were observed that fractured cohesively (Fig. 10, g–i). In particular, SCFs were torn out while the welded joints failed through the base material, indicating superior adhesive strength of the fusion zones.

Fig. 11 shows SEM micrographs of the structure of the welded joint formed in USW mode #2 at δ=100 μm and t_{USW}=800 ms. A region located to the left of the center was characterized by partial melting of the ED, as pores were found at the interface between the adherends (Fig. 11, b), which were absent in the initial PEEK film. The ED thickness was also reduced locally, but no large discontinuities were observed in the adherends near the fusion zone (Fig. 11, a, left). Closer to the center, melting and extrusion of the ED occurred (Fig. 11, c) due to the specificity of the clamping force on the circular anvil. This process was accompanied by the formation of discontinuities/pores in heat-affected zones (HAZs) of the

adherends (Fig. 11, a, right of center). To the right of the center, one more layer of the original (unmelted) ED was observed at the interface between the adherends, the thickness of which corresponded to that of the initial PEEK film. The reason for this phenomenon was a negligible clamping force in this area due to the absence of support at the sphere periphery, so frictional heating was insufficient.

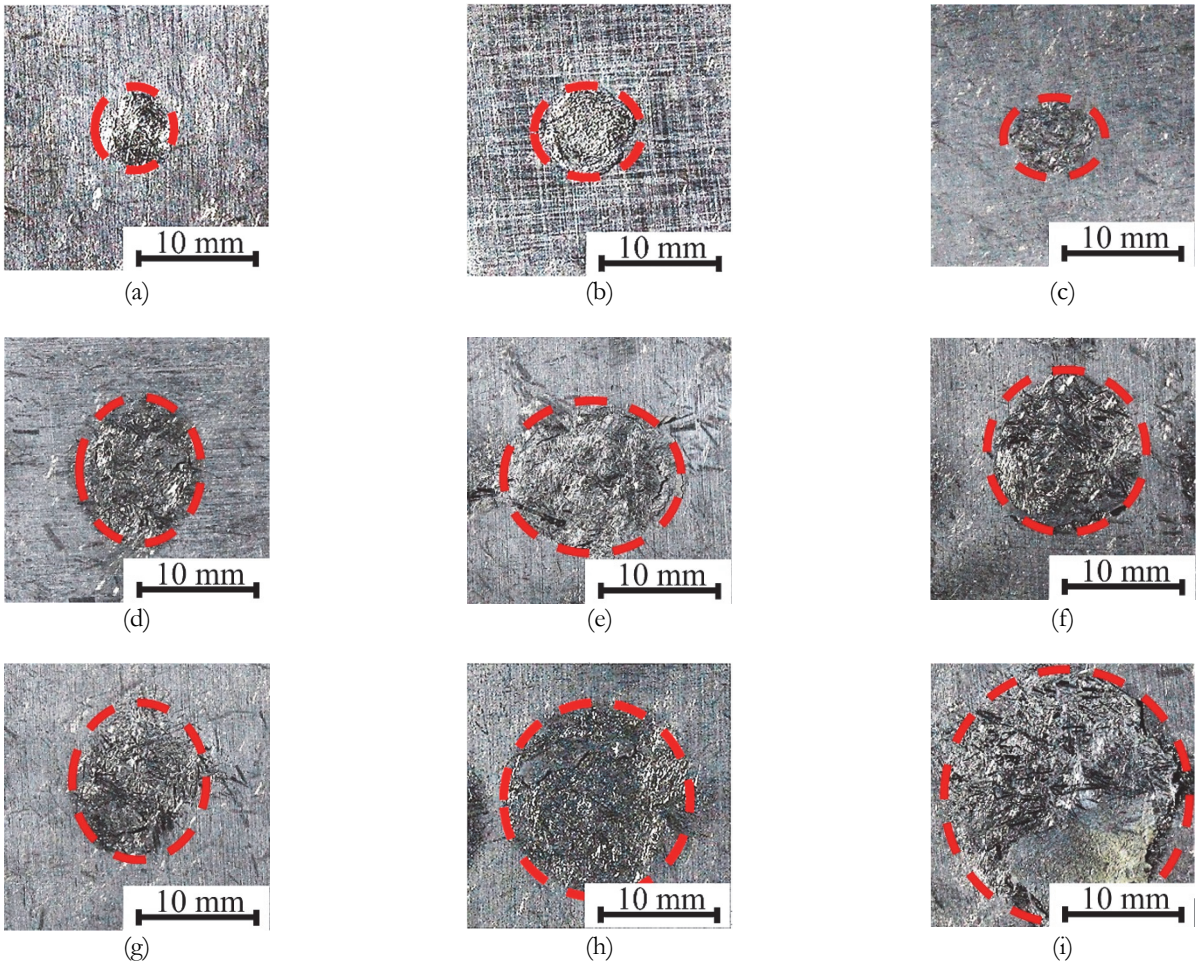

Figure 10: The OM images of the fracture surfaces; USW mode #2 without ED: a – t_{USW}=800 ms, b – t_{USW} =1000 ms, c – t_{USW} =1200 ms; ED δ=100 μm: d – t_{USW} =800 ms, e – t_{USW} =1000 ms, f – t_{USW} =1200 ms; ED δ=250 μm: g – t_{USW} =800 ms, h – t_{USW} =1000 ms, i – t_{USW} =1200 ms.

At δ=250 μm (Fig. 12), a structure similar to that described above was found. In the center of the USW-joint, the ED was melted and extruded; its flows resulted in the formation of pores (Fig. 12, c). HAZs in the adherends were characterized by some discontinuities (Fig. 12, a, center). At distances of 3–4 mm to the left, the ED was melted minimally since it was clearly detected at the interface (Fig. 12, b). As expected, the adherends were not damaged (Fig. 12, a, left). Further from the center, where the molten matrix was extruded (in addition to the ED) from the central part of the fusion zone, the structure was not uniform and contained pores (Fig. 12, a, right). Near the fusion zone, the number of discontinuities was minimal. Finally, at distances of >4 mm from the center, the original (unmelted) ED also maintained its integrity (Fig. 12, d). The reason was the same, namely the insufficient clamping force in the USW process that minimized/eliminated the possibility of its melting. Thus, under the same USW conditions, the length of the zone of complete melting of the thick ED (δ=250 μm) was >8 mm, while it was approximately two times shorter (~4 mm) at δ=100 μm.

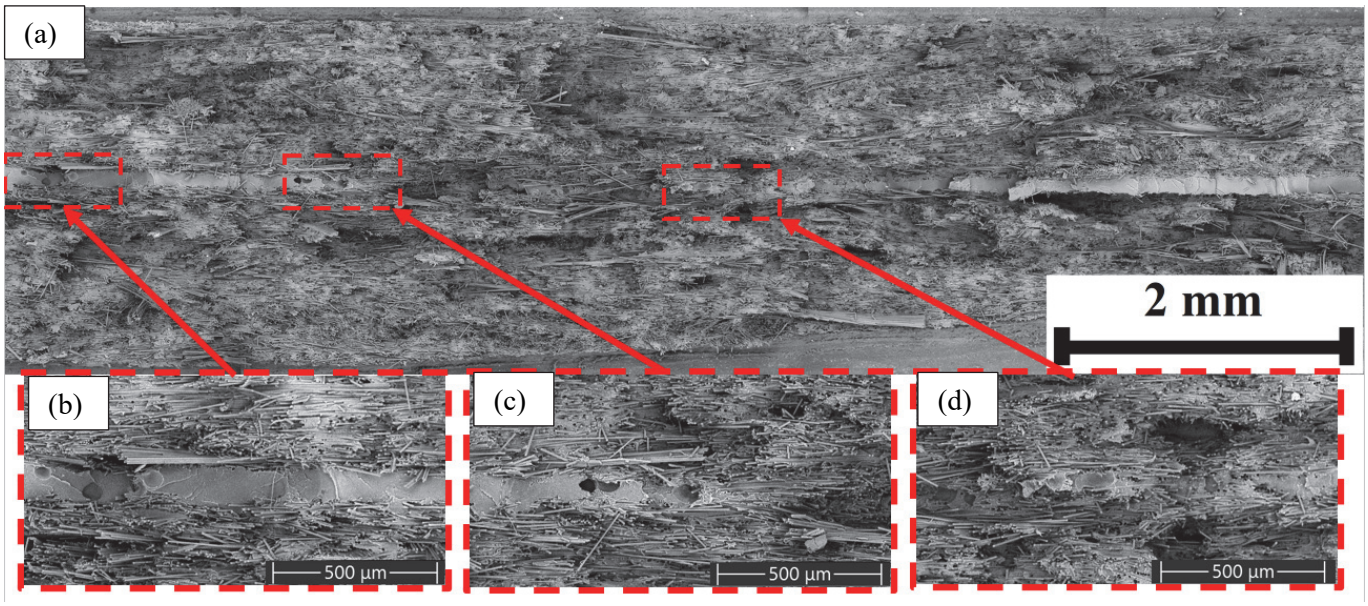

Figure 11: The SEM micrographs of the structure of the USW joint at δ=100 µm and t_{USW}=800 ms; USW mode #2.

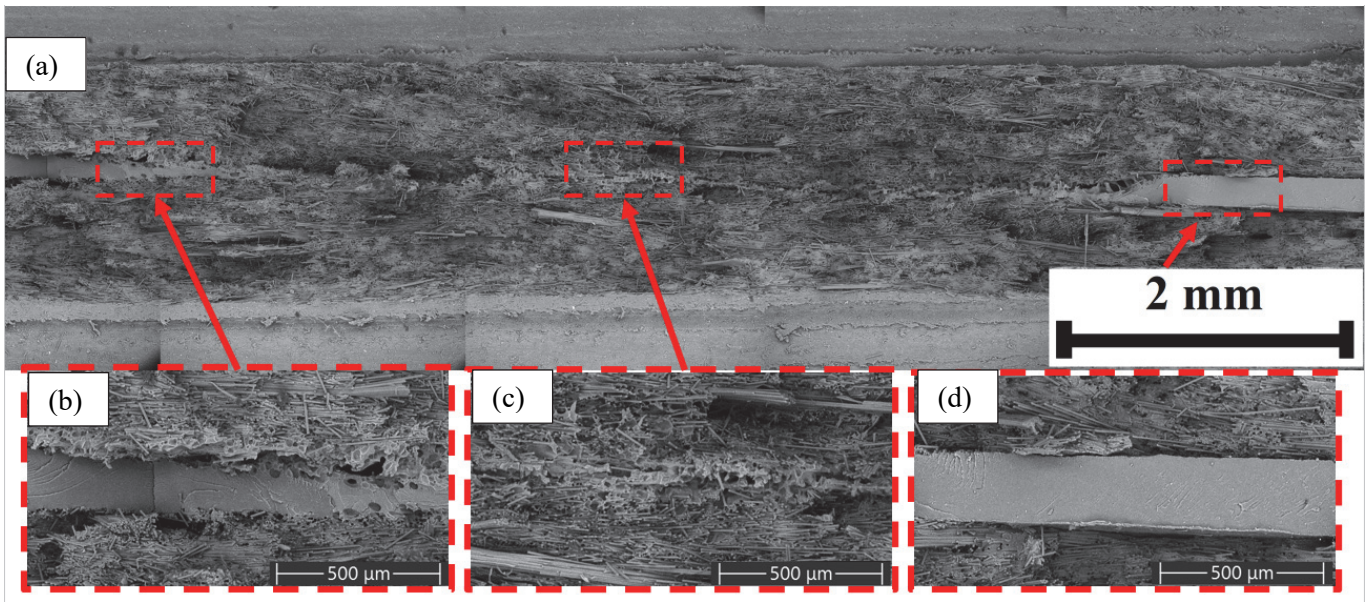

Figure 12: The SEM micrographs of the structure of the USW-joint at δ=250 µm and t_{USW}=800 ms; USW mode #2.

Discussion

The null hypothesis on complete melting and extrusion of the EDs from the fusion zones corresponding to the sonotrode area during USW was not confirmed. The limited melting pattern was caused by the negligible amplitude of US-vibrations (10 µm), which, however, did not prevent the formation of the welded joints. For USW mode #1 (t_{USW}=800 ms, δ=100 µm), the effective fusion zone area was 250 mm², or 62.5 % of the contact region, ensuring high mechanical properties (the load at failure of 4500 N and the LSS value of >11 MPa).

According to [26, 27], the amplitudes of US-vibrations could reach 80 µm with a typical level of ~30 µm. Nevertheless, previous studies were primarily focused on USW of high-strength laminates (reinforced with biaxial fabrics or unidirectional continuous CFs), so complete melting of EDs was an important condition for the formation of homogeneous structures and high strength properties of those USW-joints. In turn, they could be worsened if the surface layers of adherends melted in addition to the EDs, damaging the reinforcing fillers inside them.

Fig. 13 shows schematic representations of the formation mechanisms of the welded joints with the EDs in USW. For polymers and their composites, a typical fusion zone was divided into three major parts [28]: nugget zone (NZ), TMAZ and HAZ. The dimensions and characteristics of all three parts were determined by the combinations of the applied USW process parameters and the properties of the materials being joined. In a TMAZ, a high pressure with viscoelastic and frictional heating caused intense plastic deformation that could result in both degradation of the structure and porosity [29].

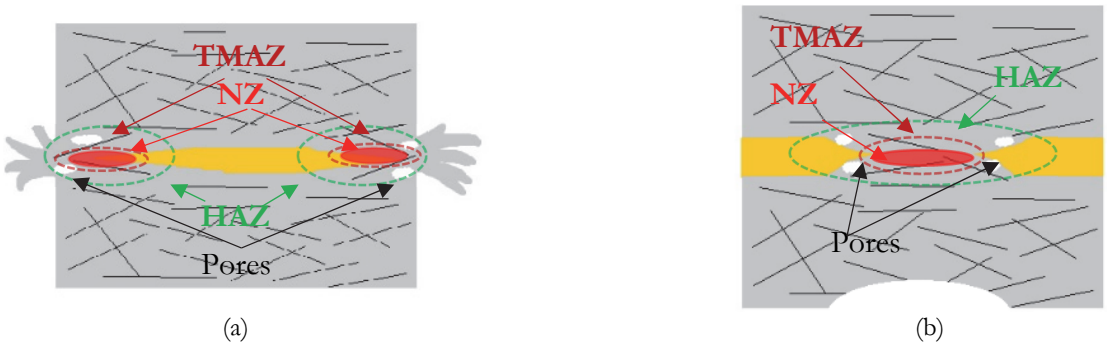

Figure 13: The schematic representations of the mechanisms of the formation of the welded joints in USW modes #1 (a) and #2 (b).

When the flat anvil was used in USW mode #1 (Fig. 13, a), primary heating and melting were concentrated at the edges of the adherends, while their central parts were subject to significantly less thermal effect. The predominance of heating at the periphery of the fusion zones was caused by less constraint conditions and, consequently, more intense frictional heat generation in these areas. So, structural inhomogeneities were observed across the entire contact regions, emphasizing the importance of the shape and size of the support in the formation of the welded joints.

The use of the spherical anvil drastically changed the pattern of the formation of the welded joints in USW mode #2 (Fig. 13, b), as it concentrated heat generation in the center of the contact regions. Consequently, the surface layers of the adherends melted directly at the contacts with the EDs, facilitating their spreading. As a result, the observed structures were more uniform across all the fusion zones, even with the lower energy input (compared to the USW mode #1).

Since USW mode #2 was aimed at the development of production routes involving the formation of a sequential series of spot-welded joints, such experiments were conducted next. Similar to the previous case, the spherical anvil was used at the USW duration of 800 ms and the clamping force of 1 atm. The variable parameters were the ED thicknesses and the distances between adjacent spots (2 mm at δ=100 μm in contrast to 4 mm for the welded joints without EDs and at δ=250 μm).

Tab. 2 presents the results of the LSS tests, as well as the measured fusion zone areas (based on the data shown in Fig. 14). The multi-spot-welded joints formed without EDs were characterized by the highest LSS values of 30.8 MPa, which were higher by 2–3 times than those with the EDs. However, the minimum fusion zone areas of 100 mm² limited their loads at failure to 3080 N.

ED thickness, μm	LSS value, MPa	Load at failure, N	Fusion zone area, mm²
100	10.4±0.5	2440±150	235±11
250	14.8±0.7	4140±150	280±14
0 (without ED)	30.8±1.2	3080±120	100±10

Table 2: The mechanical properties and dimensions of the welded joints obtained in USW mode #3.

Fig. 14 shows OM images of the fracture surfaces, where the red dotted lines mark the total fusion zone areas while the yellow ones highlight the contours of individual NZs. Thus, the implemented USW parameters ensured the spot-to-spot expansion of the fusion zone areas (Fig. 14, left to right), similar to resistance seam welding. This pattern was observed for both ED thicknesses, but the fusion zone areas remained virtually unchanged in the USW joints without EDs (Fig. 14, c).

SEM micrographs of the structure of the welded joint formed with the ED 100 μm thick are presented in Fig. 15 that confirm its complete melting. However, some discontinuities were found in the fusion zone due to intense spreading and squeezing out of the molten ED under the clamping force. Its initially negligible thickness resulted in a shortage of the

polymer binder in the areas subsequently exposed to US-vibrations. At δ=250 μm, the ED was locally melted at the maximally clamped regions (Fig. 16). In the spaces between them, some original (unmelted) fragments were observed (with thicknesses of up to 180 μm, comparable to that of the initial PEEK film). This pattern contributed to a specific "island" (linear) structure of the fusion zone characterized by the maximum load at failure of 4140 N (Tab. 2).

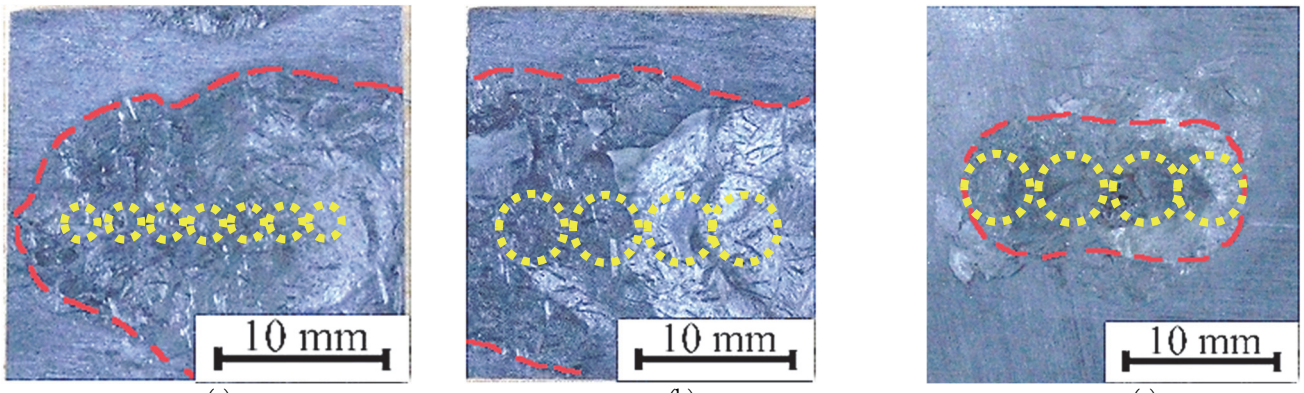

(a) (b) (c)

Figure 14: The OM images of the fracture surfaces; USW mode #3 (t_{USW}=800 ms): a – δ=100 μm, b – δ=250 μm, c – δ=0 μm (without ED).

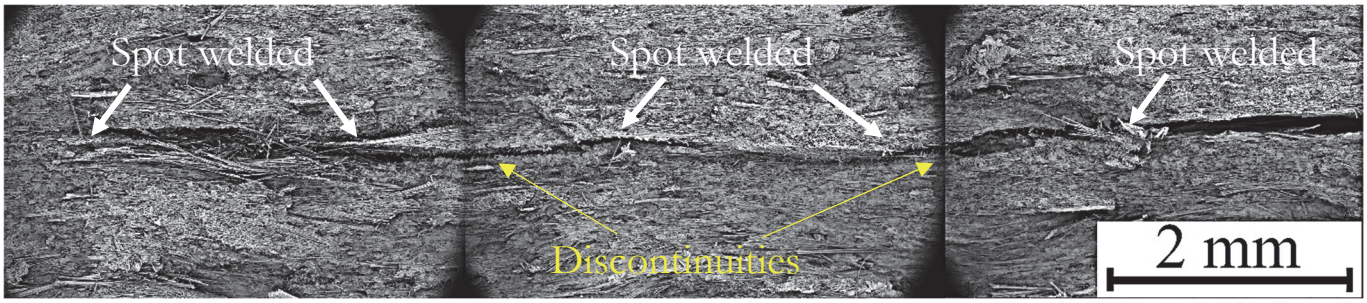

Figure 15: The SEM micrograph of the structure of the multi-spot-welded joint obtained with the ED 100 μm thick at t_{USW}=800 ms; USW mode #3.

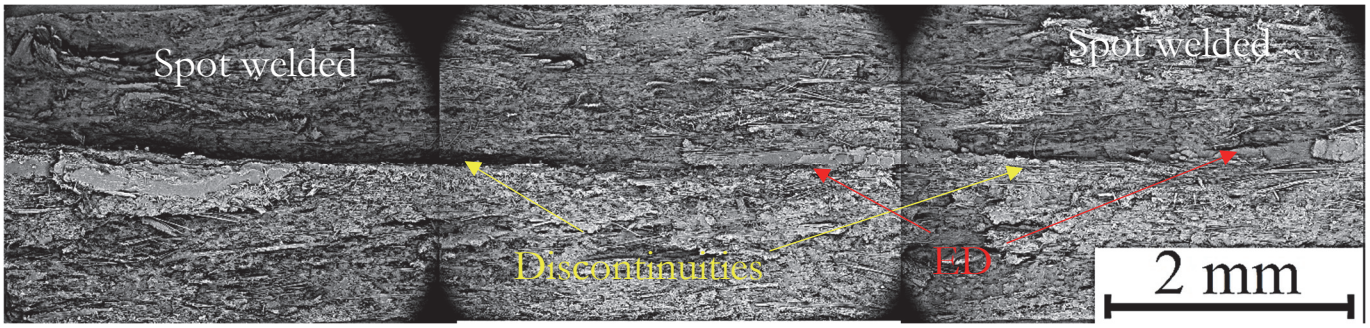

Figure 16: The SEM micrograph of the structure of the multi-spot welded joint formed with the ED 250 μm thick at t_{USW}=800 ms; USW mode #3.

With the use of the ED 100 μm thick, the multi-spot-welded joints with the short distance of 2 mm accumulated sufficient frictional heat for its complete melting and extrusion from the contact region. Due to overheating of the polymer, it was impossible to control the formation of the welded joint. Given the short distances between adjacent spots, TMAZs and HAZs overlapped, increasing partial melting of the surface layers of the adherends. However, this phenomenon was excluded by enlarging the distances between adjacent spots to 4 mm when using the 250 μm thick ED. Consequently, the island-like structure was observed, where isolated areas of the molten ED alternated with zones of the original (unmelted) polymer. Without EDs, the USW joints were formed uniformly: NZs and TMAZs were not overlapped, while the numbers of discontinuities were minimal.

Based on the above, the distances between adjacent spots should be carefully selected for such welded joints considering the ED thickness. Specifically, the following patterns were identified in this study:
- at δ=100 μm, the distances between adjacent spots should be widened to prevent overlapping of HAZs and TMAZs;
- at δ=250 μm, on the contrary, they should be shortened to ensure overlapping of NZs and eliminating island-like discontinuities of the formed structures;
- for USW without EDs, localized heating of the contact regions could be recommended, since it would keep both NZs and TMAZs "thermally isolated," enabling to maintain the structural integrity of adherends (in such cases, the distances between adjacent spots should be precisely calculated to ensure the required load-bearing capacity of welded joints).
Thus, the optimization of USW procedures for particulate PEEK/SCF composites should be aimed at achieving a balance between the distances between adjacent spots and the ED thickness to ensure control of melting the polymer in fusion zones (outside the clamped region) and to eliminate the formation of discontinuities caused by its deficiency due to melting and squeezing out.

Conclusions

During the USW of the adherends from the PEEK/SCF composite using the flat anvil (mode #1), frictional heating developed primarily along the periphery of the fusion zones due to the less constraint fixation. The rational determined parameters include the ED thickness of 100 μm and the USW duration of 800 ms, which enabled the formation of the fusion zones with the area of ~250 mm² (62.5 % of the contact region) and the LSS value of >11 MPa with the load at failure of >4500 N. The proper quality of these welded joints was confirmed by their failure through the base material (due to bending of the adherends).
The use of the spherical anvil (USW mode #2) localized frictional heating and fusion in the centers of the clamped regions. Without EDs, the welded joints achieved the maximum stresses at failure of >60 MPa, but the small fusion zone areas limited their load-bearing capacities to 3000 N. With the ED 100 μm thick at t_{USW}=1000 ms, the LSS value was about 52 MPa, but the load al failure increased up to 4900 N. The maximum load-bearing capacity of >6000 N was recorded with the thickest ED of 250 μm at the "moderate" LSS value of ~40 MPa due to the largest fusion zone area.
The multi-spot-welded joints of the adherends from the PEEK/SCF composite formed without EDs were characterized by the structural integrity at the stress at failure of ~30.8 MPa, which was 2–3 times higher than those with the EDs 100 and 250 μm thick. The quality of the multi-spot-welded joints was determined by the ratio of the ED thickness to the distances between adjacent spots. Inserting the EDs significantly enlarged the fusion zone areas, but uneven distributions of US-vibrations within the clamped region resulted in different EDs' melting and spreading patterns, leading to inhomogeneities/discontinuities in the formed structures.
The optimization of USW procedures for fibrous PEEK/SCF composites should be aimed at achieving a balance between the distances between adjacent spots and the ED thickness to ensure control of melting the polymer in fusion zones (outside the clamped region) and to eliminate the formation of discontinuities caused by its deficiency due to squeezing out.

Acknowledgments

The study was funded by the 24-79-00189 grant from the Russian Science Foundation. https://rscf.ru/project/24-79-00189. The SEM examinations were performed using equipment of the Nanotech shared use center of the Institute of Strength Physics and Materials Science SB RAS and core facility "Structure, mechanical and physical properties of materials" of NSTU.

References

[1] Ramya, U., Sammaiah, P., Kumar, K.S. (2025). Scientometric analysis of CF-PEEK composites: Research trends and emerging opportunities, Next Res., 2(3), pp. 100513. DOI: https://doi.org/10.1016/j.nexres.2025.100513.
[2] Dong, W., Karalis, G., Liebscher, M., Wang, T., Liu, P., Li, W. and Mechtcherine, V. (2025). Multifunctional carbon fibre reinforced polymer (CFRP) composites for sustainable and smart civil infrastructure: A comprehensive review, Sustainable Mater.Technol., 45, pp. e01594. DOI: https://doi.org/10.1016/j.susmat.2025.e01594.

[3] Qiu, P., Bennani, V., Cooper, P., Dias, G., Ratnayake, J. (2024). Surface chemistry on PEEK surfaces: From enhanced biofunctionality to improved surface modifiability, Appl. Mater. Today., 41, pp. 102523. DOI: https://doi.org/10.1016/j.apmt.2024.102523.
[4] Babaci, A.M., Nurbaş, M. (2026). Polyetheretherketone (PEEK): A Comprehensive Review of Advanced Polymer Engineering, Biomedical Applications, and Emerging Technological Frontiers, Gazi Univ. J. Sci. Part A: Eng. Innov., 13(1), pp. 483–521. DOI: https://doi.org/10.54287/gujsa.1870133.
[5] Yan, M., Tian, X., Yao, R. (2022). Processability and reusability of CF/PEEK mixture for Powder Bed Fusion of high strength composites, Compos. Commun., 35, pp. 101318. DOI: https://doi.org/10.1016/j.coco.2022.101318.
[6] Khatri, B., Roth, M. F., and Balle, F. (2022). Ultrasonic Welding of Additively Manufactured PEEK and Carbon-Fiber-Reinforced PEEK with Integrated Energy Directors. Journal of Manufacturing and Materials Processing, 7(1), pp. 2. DOI: https://doi.org/10.3390/jmmp7010002.
[7] Bonmatin, M., Chabert, F., Bernhart, G., Cutard, T., and Djilali, T. (2022). Ultrasonic welding of CF/PEEK composites: Influence of welding parameters on interfacial temperature profiles and mechanical properties. Composites Part A: Applied Science and Manufacturing, 162, pp. 107074. DOI: https://doi.org/10.1016/j.compositesa.2022.107074.
[8] Tsiangou, E.; Teixeira de Freitas, S.; Villegas, I.F.; Benedictus, R. (2020) Ultrasonic welding of epoxy- to polyetheretherketone- based composites: Investigation on the material of the energy director and the thickness of the coupling layer. J. Compos. Mater., 54, pp. 3081–3098. DOI: https://doi.org/10.1177/0021998320910207.
[9] Wang, J., Lu, C., Xiao, C., Cheng, J., Ren, R., and Xiong, X. (2023). Heat distribution simulation and effects of ultrasonic welding amplitude on carbon fiber/polyetherimide composite joint properties. Materials Letters, 340, pp. 134148. DOI: https://doi.org/10.1016/j.matlet.2023.134148.
[10] Oliveira, P. R., Virgen, G. P. G., Imbert, M., Beisel, S., May, M., Panzera, T. H., Hiermaier S. and Balle, F. (2023). Ultrasonically welded eco-friendly sandwich panels based on upcycled thermoplastic core: An eco-mechanical characterisation. Resources, Conservation & Recycling Advances, 20, pp. 200187. DOI: https://doi.org/10.1016/j.rcradv.2023.200187.
[11] Tsiangou, E., Kupski, J., Teixeira de Freitas, S., Benedictus, R. and Villegas, I.F. (2021). On the sensitivity of ultrasonic welding of epoxy- to polyetheretherketone (PEEK)-based composites to the heating time during the welding process, Compos. A Appl. Sci. Manuf.,144, pp. 106334. DOI: https://doi.org/10.1016/j.compositesa.2021.106334.
[12] Alexenko, V.O. and Panin, S.V. (2025). The effect of energy director on ultrasonic consolidation of multilayered composites (laminates) made from unidirectional PEEK/CF prepregs, Frat. Integrità Strutt., 20(75), pp. 315–325. DOI: https://doi.org/10.3221/IGF-ESIS.75.22.
[13] Yuan, J., Xiao, H., Wang, Y., Cui, W., Duan, Y., Xin, Z., Wang, B. (2026). Ultrasonic welding process and strategies for performance regulation of Fiber reinforced thermoplastic composites: A review, J. Manuf. Process., 157, pp. 531–553. DOI: https://doi.org/10.1016/j.jmapro.2025.11.084.
[14] Wang, Y., Rao, Z., Liao, S., Wang, F. (2021). Ultrasonic welding of fiber reinforced thermoplastic composites: Current understanding and challenges, Compos. Part A Appl. Sci. Manuf., 149, pp. 106578. DOI: https://doi.org/10.1016/j.compositesa.2021.106578.
[15] Bose, S., Chelladurai, H. and Ponappa, K. (2024). A review on recent developments in ultrasonic welding of polymers and polymeric composites, Weld. World., 68, pp. 1881–1903. DOI: https://doi.org/10.1007/s40194-024-01693-w.
[16] Khatri, B., Roth, M. and Balle, F. (2023). Ultrasonic welding of additively manufactured PEEK and carbon-fiber-reinforced PEEK with integrated energy directors, J. Manuf. Mater. Process., 7(1), pp. 2. DOI: https://doi.org/https://doi.org/10.3390/jmmp7010002.
[17] Wang, T., Shi, R., Liu, Z., Ao, S., Luo, Z., Wang, K., Li, Y. (2024). Effect of ultrasonic embossing and welding time on the joint performance of ultrasonically welded short carbon fiber reinforced PEEK, J. Mater. Res. Technol., 28, pp. 3258–3266. DOI: https://doi.org/10.1016/j.jmrt.2023.12.266.
[18] Liu, Y., Li, J. and Wu, Z. (2025). Ring-Focused Ultrasonic Welding of CF/PEEK Composites Without Energy Director, J. Mater. Eng. Perform., 35, pp. 3850–3862. DOI: https://doi.org/10.1007/s11665-025-11865-4.
[19] Yang, Y., Li, Y. Liu, Z., Li, Y., Ao S., Luo Z. (2022). Ultrasonic welding of short carbon fiber reinforced PEEK with spherical surface anvils, Compos. B Eng., 231, pp. 109599. DOI: https://doi.org/10.1016/j.compositesb.2021.109599.
[20] Brito, C. B. G., Teuwen, J., Dransfeld, C.A. and Villegas, I. F. (2025). Ultrasonic welding of thermoplastic composites: A comparison between polyetheretherketone and low-melt polyaryletherketone as resin in the adherends and energy directors, Compos. B Eng., 296, pp. 112264. DOI: https://doi.org/10.1016/j.compositesb.2025.112264.
[21] Tian, D., Alexenko, V.O., Panin, S.V., Bogdanov, A.A., Buslovich, D.G. (2024). Effect of the Energy Director Material on the Structure and Properties of Ultrasonic Welded Lap Joints of PEI Plates with CF Fabric/PEI Prepreg, J. Compos. Sci., 8(4), pp. 150. DOI: https://doi.org/10.3390/jcs8040150.

[22] Bhudolia, S. K., Gohel, G., Leong, K. F. and Islam, A. (2020) Advances in ultrasonic welding of thermoplastic composites: a review, Materials, 13(6), pp. 1284–1310. DOI: https://doi.org/10.3390/ma13061284.
[23] Alexenko, V.O., Panin, S.V., Stepanov, D.Y., Byakov, A.V., Bogdanov, A.A., Buslovich, D.G., Panin, K.S., Tian, D. (2023). Ultrasonic Welding of PEEK Plates with CF Fabric Reinforcement–The Optimization of the Process by Neural Network Simulation, Materials, 16, pp. 2115. DOI: https://doi.org/10.3390/ma16052115.
[24] Bonmatin, M., Chabert, F., Bernhart, G., Cutard, T., Djilali, T. (2022). Ultrasonic welding of CF/PEEK composites: Influence of welding parameters on interfacial temperature profiles and mechanical properties, Compos. Part A Appl. Sci. Manuf., 162, pp. 107074. DOI: https://doi.org/10.1016/j.compositesa.2022.107074.
[25] Villegas, I. F. and van Moorlegled, R. (2018). Ultrasonic welding of carbon/epoxy and carbon/PEEK composites through a PEI thermoplastic coupling layer, Compos. A Appl. Sci. Manuf., 109, pp. 75–83. DOI: https://doi.org/10.1016/j.compositesa.2018.02.022.
[26] Wang, X., Quan, D., Liu, J., Yue, D., Pan, J., Zhao, G. (2025). Towards ultrasonic welding of robust thermoplastic composite joints without the use of energy directors, Compos. Part B-Eng., 302, pp. 112561. DOI: https://doi.org/10.1016/j.compositesb.2025.112561.
[27] Villegas, I. F. (2014). Strength development versus process data in ultrasonic welding of thermoplastic composites with flat energy directors and its application to the definition of optimum processing parameters, Compos. A Appl. Sci. Manuf., 65, pp. 27–37. DOI: https://doi.org/10.1016/j.compositesa.2014.05.019.
[28] Cui, Y., Zhang, T., Xing, Y., Liang, J. (2025). Ultrasonic spot welding of dissimilar short- and continuous-fiber reinforced PA6 composites: Fiber redistribution, porosity formation, and joint strengthening mechanisms, J. Manuf. Process., 154, pp. 150–164. DOI: https://doi.org/10.1016/j.jmapro.2025.09.078.
[29] Panin, S.V., Bogdanov, A.A., Alexenko, V.O., Bochkareva, S.A., Lyubutin, P.S., Panov, I.L., Tian, D. (2024). Digital Image Correlation Analysis of Fatigue Degradation of Layered Polymer Composites (Polyetheretherketone/Polyetherimide, PEEK/PEI) with Carbon-Fiber Fabric Prepreg, Phys. Mesomech., 27(5), pp. 541–555. DOI: https://doi.org/10.1134/S1029959924050047.

NOMENCLATURE

ED - energy director
HAZ - heat-affected zone
LSS - interlaminar shear strength
NZ - nugget zone
OM -optical microscope
PEEK - polyetheretherketone
PMC - polymer matrix composite
SEM - scanning electron microscope
SCF - short carbon fibers
TMAZ - thermomechanically affected zone
USW - ultrasonic welding
δ [μm] - ED thickness
t_{USW} [ms] - USW duration
P [N] - Load at failure
F [mm^2] - Contact area of the joined adherends